Elucidating deactivation of titania-supported cobalt Fischer-Tropsch catalysts under simulated high conversion conditions

van Koppen, Luke M.; Iulian Dugulan, A.; Leendert Bezemer, G.; Hensen, Emiel J.M.

DOI
10.1016/j.jcat.2023.02.019

Publication date
2023

Document Version
Final published version

Published in
Journal of Catalysis

Journal of Catalysis 420 (2023) 44–57

Contents lists available at ScienceDirect

Journal of Catalysis

journal homepage: www.elsevier.com/locate/jcat

Elucidating deactivation of titania-supported cobalt Fischer-Tropsch catalysts under simulated high conversion conditions

Luke M. van Koppen [a,b], A. Iulian Dugulan [b], G. Leendert Bezemer [c], Emiel J.M. Hensen [a,*]

[a] Laboratory of Inorganic Materials and Catalysis, Department of Chemical Engineering and Chemistry, Eindhoven University of Technology, Het Kranenveld, 14 5600 MB Eindhoven, the Netherlands

[b] Laboratory of Fundamentals Aspects of Materials and Energy, Department of Radiation Science & Technology, Delft University of Technology, Mekelweg 15, 2628 CD Delft, the Netherlands

[c] Energy Transition Campus Amsterdam, Shell Global Solutions International B.V., Grasweg 31, 1031 HW Amsterdam, the Netherlands

ARTICLE INFO

Article history:
Received 27 December 2022
Revised 14 February 2023
Accepted 22 February 2023
Available online 26 February 2023

Keywords:
Fischer-Tropsch synthesis
Cobalt
Humidity
Deactivation
Mössbauer spectroscopy

ABSTRACT

The study of titania-supported cobalt nanoparticles is relevant for industrial Fischer-Tropsch synthesis (FTS). Herein, we report about various deactivation pathways of cobalt supported on P25 titania (cobalt loading 2–8 wt%) under simulated high conversion conditions using *in situ* Mössbauer spectroscopy. A fraction of metallic cobalt was oxidized under humid FTS conditions. The absolute amount of oxidized cobalt was ~ 1.2 wt% independent of the cobalt loading, indicating that specific cobalt-titanol interactions are involved in the oxidation process. The formation of cobalt-titanate-like compounds was only observed under very high water-to-hydrogen ratios in the absence of carbon monoxide. Steam considerably enhances cobalt sintering under FTS conditions. As such, deactivation under humid FTS conditions is not only caused by cobalt oxidation but also by enhancing sintering of the active phase.

1. Introduction

Fischer-Tropsch synthesis (FTS) is a surface-catalyzed polymerization reaction that converts a feed of synthesis gas ($CO + H_2$) to fuels and chemicals [1]. Cobalt catalysts are preferred in industry when the synthesis gas is derived from natural gas and long-chain paraffins are targeted [2]. Structure sensitivity of the FTS reaction catalyzed by cobalt dictates that the optimum size of cobalt nanoparticles is around 6–8 nm [3,4]. As such, it is important to understand the stability of cobalt nanoparticles for successful industrial applications [5].

One can distinguish short- and long-term deactivation of the catalyst in cobalt-based FTS [6]. Short-term deactivation is well studied [5,7,8] and can be reversed by mild hydrogen treatment [9]. Long-term deactivation, on the other hand, is less reversible, making it significant in industrial practice. Long-term deactivation is not well understood, and several factors can contribute to the loss of catalytic activity over time. The most common ones considered are oxidation of the active metal phase [10–13], strong-metal support interactions (SMSI) [14–16], carbon deposition [17–19] and cobalt sintering [20–22].

Investigations on supported cobalt catalysts are typically done using irreducible oxide supports such as SiO_2 [16,23,24] and Al_2O_3 [2,25,26]. Reducible oxides such as TiO_2, are also of practical interest [27–30]. The support reducibility can result in the formation of cobalt-support compounds [31,32]. The formation of such compounds can lead to significant irreversible deactivation.

Water is a main product of the FTS reaction, because the main pathway for O removal from the surface upon CO dissociation is through the production of water. High partial pressures of steam (humidity) can result in deactivation through oxidation as well as enhanced sintering. Thermodynamics dictate that spherical cobalt nanoparticles smaller than about 4 nm oxidize relevant H_2O/H_2 ratios during FTS conditions [11]. However, bulk oxidation of supported cobalt catalysts under such (simulated) industrial FTS conditions is often not observed in experiments, which can be due to the fact that typical catalysts contain larger particles or due to kinetic limitations of water dissociation [5,10,13,33,34]. The effect of steam on sintering under FTS conditions has been investigated [21,34,35]. The combination of high partial pressure of steam and carbon monoxide accelerates agglomeration of the active metal phase. The exact mechanisms at play are still a matter of discussion. Kliewer et al. proposed that surface wetting by cobalt oxide/hydroxide species forms a bridge between metallic particles that promotes coalescence [29]. With the size of such bridges lim-

* Corresponding author.
E-mail address: e.j.m.hensen@tue.nl (E.J.M. Hensen).

https://doi.org/10.1016/j.jcat.2023.02.019
0021-9517/

ited by the metallic particle size, indicating that initial dispersion is key to resisting water induced sintering. Moodley et al. suggested Ostwald ripening by sub-carbonyl species as the dominant mechanism, which is enhanced by the presence of water [7].

In this work, we investigate the deactivation pathways of titania-supported cobalt catalysts under humid FTS and model oxidation conditions. The chemical state of cobalt is investigated under conditions close to those encountered in industrial practice using *in situ* Mössbauer emission spectroscopy (MES) [36]. Here, we expand on previous ^{57}Co MES studies that showed the effect of steam on the sintering of cobalt catalysts supported on carbon nanofibers [34,35] by studying cobalt supported on a titania support. The MES measurements are supplemented by ICP, XRD, TEM and STEM-EDX, while the catalytic performance was determined during the MES measurements as well as separately in a microflow reactor.

2. Experimental methods

2.1. Catalyst preparation

Supported cobalt catalysts were prepared by incipient wetness impregnation of P25 titania (Evonik Degussa, pore volume 0.3 mL/g, BET surface area 50 m^2/g, Anatase/Rutile 85:15) followed by drying in air at 120 °C for 6 h. The impregnation solutions were obtained by dissolving the appropriate amount of $Co(NO_3)_2{\cdot}6H_2O$ (≥98.0 %, Sigma Aldrich) in dehydrated ethanol. Four catalysts were prepared with a cobalt loading between 2 and 8 wt%. The resulting samples are denoted by Co(x)/TiO_2, where × represents the intended weight loading. Two more catalysts were later prepared for additional studies following the same approach. Following impregnation and drying, the samples were calcined at 350 °C for 2 h in stagnant air (rate 5 °C/min). Part of these prepared catalysts was spiked with radioactive ^{57}Co by pore volume impregnation using a solution containing 90 MBq ^{57}Co in 0.1 M HNO_3. These radioactive samples were dried at 120 °C for 12 h and subsequently used for Mössbauer spectroscopy.

2.2. Characterization

2.2.1. Inductively coupled plasma-optical emission spectrometry

Inductively coupled plasma-optical emission spectrometry (ICP-OES) spectrometer (Spectroblue, AMETEK Inc.) was used for elemental analysis. For analyzing the cobalt content of the catalysts, approximately 25 mg of the sample was dissolved in a mixture of 2 mL of concentrated HNO_3 (65 %) and 5 mL of concentrated H_2SO_4 (95–98 %). The mixture was heated by a heating plate set to 250 °C until fully dissolved. After cooling to room temperature, demineralized water was added through a reflux and homogenized. The solutions were subsequently diluted for ICP-OES measurements with demineralized water using volumetric flasks. ICP-OES analysis was conducted in duplo. A calibration line was prepared using a standard Co solution with concentrations between 0 and 6 mg/L. The cobalt concentration was determined using the 228.616 and 238.892 nm wavelengths and the average was reported.

2.2.2. X-ray diffraction

X-ray diffraction (XRD) patterns were recorded on a Bruker D2 Phaser using a Cu Kα radiation source and a 2 mm slit. Data was collected using a time per step of 0.15 min and a step size of 0.1° in the 2θ range of 10–60°. Background subtractions were applied, and reference spectra were obtained using the Diffrac.Eva software by Bruker.

2.2.3. Electron microscopy

Surface averaged particle sizes and particle size distributions were determined using transmission electron microscopy (TEM). TEM measurements were performed on a FEI Tecnai 20 electron microscope operated at an electron acceleration voltage of 200 kV with a LaB6 filament. Typically, a small amount of the sample was ground and suspended in pure ethanol, sonicated, and dispersed over a Cu grid with a holey carbon film.

The nanoscale distribution of elements in the samples was studied using scanning transmission electron microscopy – energy-dispersive X-ray spectroscopy (STEM-EDX). Measurements were carried out on a FEI cubed Cs-corrected Titan operating at 300 kV. Samples were crushed, sonicated in ethanol, and dispersed on a holey Cu support grid. Elemental analysis was done with an Oxford Instruments EDX detector X-MaxN 100TLE.

2.2.4. In situ Mössbauer emission spectroscopy

Mössbauer emission spectroscopy (MES) was carried out at various temperatures using a constant acceleration spectrometer set up in a triangular mode with a moving single-line $K_4Fe(CN)_6{\cdot}3H_2O$ absorber enriched in ^{57}Fe. The velocity scale was calibrated with a ^{57}Co:Rh source and a sodium nitroprusside absorber. Zero velocity corresponds to the peak position of the $K_4Fe(CN)_6{\cdot}3H_2O$ absorber measured with the ^{57}Co:Rh source, positive velocities correspond to the absorber moving towards the source. To be able to measure under *in situ* Fischer-Tropsch conditions, a high pressure MES cell is used [36], which is described in detail in literature [35].

Mössbauer spectra were fitted using the MossWinn 4.0 program [37]. The spectra of very small superparamagnetic species were fitted using the two-state magnetic relaxation model of Blume and Tjon, which assumes the presence of a fluctuating magnetic field which jumps between the values of + H and -H along the *z*-axis with an average frequency τ [38]. Here, H typically equals 500 kOe and τ can vary between 10^{-9} and 10^{-12} s^{-1}. The Mössbauer spectra of larger particles were fitted using a hyperfine sextuplet, resulting from the local magnetic field experienced by bulk metallic particles. The experimental uncertainties in the calculated Mössbauer parameters, estimated using Monte Carlo iterations by the MossWinn 4.0 program and including experimental uncertainties were as follows: IS and QS ± 0.01 mm s^{-1} for the isomer shift and quadrupole splitting, respectively; ± 3 % for the spectral contribution; ± 3 kOe for the hyperfine field.

Typically, 300 mg of radioactivity-spiked and 100 mg of non-radioactive catalyst (sieve fraction 250–500 μm) was loaded into two separate compartments of the reactor cell. FTS experiments were performed *in situ* following reduction at 340 °C for 2 h in 100 mL/min flow of pure H_2. Reactions were done at 200 °C and 20 bar, while the H_2/CO was kept at 4 throughout and steam was fed to vary the relative humidity. Water was evaporated and mixed with the incoming feed gas using a Bronkhorst controlled evaporator mixer (CEM). The reported relative humidity are determined solely by the fed steam, excluding the steam produced by the Fischer-Tropsch reaction. Wax products were collected in a downstream hot catch pot, and water was retrieved in a subsequent cold catch pot. An online Trace GC Ultra from Thermo Fisher Scientific equipped with a RT-Silica bond column and a flame ionization detector as well as a Stabilwax column and a thermal conductivity detector was used to analyse the gaseous products. Model oxidation experiments were performed *in situ* following a reduction treatment at 340 °C for 2 h in 100 mL/min of pure H_2. Such reactions were done at a temperature of 220 °C and a pressure of 20 bar with a constant relative humidity (RH) of 25 % and a varying H_2 partial pressure.

2.3. Catalytic activity measurements

The catalytic performance was determined in a single-pass flow reactor system (Microactivity Reference unit, PID Eng&Tech) operated at a temperature of 220 °C or 240 °C, a total pressure of 20 bar and a H_2/CO ratio of 4. In a typical experiment, 50 mg of catalyst (sieve fraction 125–250 μm) mixed with SiC particles of the same sieve fraction to a total volume of 3 mL was placed in a tubular reactor with an internal diameter of 9 mm. The temperature was controlled via a thermocouple, located in the centre of the catalytic bed. Reduction was first performed in a flow of H_2 at 350 °C for 2 h after heating at a rate of 5 °C/min. Subsequently, the reactor was cooled to 220 °C and the gas feed composition was changed to reaction conditions. A constant space velocity (SV) of 60 L $g_{cat}^{-1}h^{-1}$, was applied for all catalysts, which resulted in a CO conversion between 1 and 5 %. A TRACE1300 GC instrument from Thermo Fisher Scientific equipped with a RT-Silica bond column and a flame ionization detector as well as a Porabond-Q column and a thermal conductivity detector was used to measure the gas composition of the reactor effluent. The Weisz – Prater criterion was calculated to confirm operations did not run under internal mass transfer limitations. At the applied reaction conditions, no CO_2 was observed and the selectivity toward oxygenates on a molar carbon basis was less than 1 %. Liquid products and waxes were collected in a cold trap placed after the reactor. Ar was used an internal standard in the CO/H_2 feed mixture. The CO conversion (X_{CO}) was determined in the following manner:

$$X_{CO} = 1 - \frac{F_{Ar,in}F_{CO,out}}{F_{CO,in}F_{Ar,out}} \quad (1)$$

where $F_{Ar,in}$ is the volumetric Ar flow in the reactor feed, $F_{CO,in}$ is the volumetric CO flow in the reactor feed, $F_{Ar,out}$ and $F_{CO,out}$ are the respective volumetric flows of Ar and CO out of the reactor system.

The carbon-based selectivity of hydrocarbon compound C_i (S_{Ci}) was calculated using:

$$S_{Ci} = \frac{F_{Ar,in}F_{Ci}\nu_i}{F_{Ar,out}F_{CO,in}X_{CO}} \quad (2)$$

where F_{Ci} is the volumetric flow of hydrocarbon compound C_i out of the reactor, and ν_i is the stochiometric factor of the hydrocarbon compound.

The cobalt time-yield (CTY) was determined using the following equation:

$$CTY = \frac{F_{CO,in}X_{CO}}{m_{Co}} \quad (3)$$

where m_{Co} is the weight of cobalt used in the catalytic reaction determined through ICP analysis.

3. Results and discussion

3.1. Fresh catalyst characterization

A set of four Co/TiO_2 catalysts was prepared by incipient wetness impregnation with intended cobalt loadings of 2, 4, 6 and 8 wt%. The actual cobalt loadings determined by ICP analysis are given in Table 1, which point to some deviations from the targeted values.

Table 1
Cobalt loading and average metal particle of Co/TiO_2 catalysts.

Catalyst	Co loading (wt%)[a]	Particle size (nm)[b]
Co(2)/TiO_2	3.0	13.3 ± 6.4
Co(4)/TiO_2	5.0	13.4 ± 6.6
Co(6)/TiO_2	5.6	12.0 ± 4.8
Co(8)/TiO_2	7.4	11.0 ± 4.6

[a] Determined by ICP analysis.
[b] Determined by TEM analysis of reduced and passivated samples.

Fig. 1 shows representative TEM images of the catalysts after reduction at 340 °C for 2 h in pure H_2 and subsequent passivation at room temperature in a flow of 5 % O_2 in He. The average size and size distribution of the cobalt nanoparticles was determined by analysing approximately 150 particles in ca. 8 images per sample. The TEM images show that cobalt is well dispersed over the surface in all catalysts without any large agglomerated forms of cobalt. The average particle sizes given in Table 1 show that the size of the reduced cobalt particles does not depend on the cobalt loading within the accuracy limits. This agrees with findings reported by Van Deelen et al. [39] that reduction of size-controlled cobalt particles, which were obtained through colloidal methods and loaded on P25 titania by impregnation, leads to nearly similar sizes of the final metallic cobalt particles.

The X-ray diffractograms of the calcined precursors are given in Fig. 2. The samples show only diffraction lines due to anatase and rutile TiO_2, which is expected for P25 TiO_2 [40]. Features due to cobalt oxide are not observed, indicative of the high dispersion of cobalt oxide in the calcined precursor. The X-ray diffractograms of the reduced and passivated samples were similar to those of the calcined samples.

3.1.1. In situ Mössbauer spectroscopy of reduced catalysts

Mössbauer spectra of the catalysts after reduction at 340 °C for 2 h are given in Fig. 3. The Mössbauer fit parameters of the reduced catalysts are listed in Tables S3-S6. A sextuplet with an isomer shift (IS) of −0.1 mm s^{-1} and a hyperfine field (HF) of ∼ 323 kOe observed for all catalyst samples is due to metallic cobalt. This sextuplet points to the presence of magnetically ordered metallic cobalt particles, which is common for cobalt particles larger than 6 nm [34]. The absence of a singlet feature of superparamagnetic metallic cobalt means that the fraction of very small cobalt nanoparticles with a size smaller than 6 nm in these samples is below the detection limit. This result is in line with the TEM analysis of the reduced catalysts. This aspect is important, as it has been well established that the FTS reaction on cobalt is structure sensitive with the CO conversion strongly decreasing for particles smaller than 6 nm [4]. In addition to the dominant metallic cobalt phase, all spectra contain a doublet with an IS of 1.0 mm s^{-1} and a quadrupole splitting (QS) of 2.0 mm s^{-1}, which can be assigned to a dispersed Co^{2+}-oxide phase. The contribution of this oxidic phase is largest (47 %) for Co(2)/TiO_2. When the reduction is prolonged to 10 h, the oxide phase spectral contribution decreased to 22 %. The requirement of a longer reduction is likely the result of the increased cobalt-titania interaction on this sample, and the reduced hydrogen spill over from metallic cobalt particles onto the support. The catalysts with a higher cobalt loading have a smaller contribution of cobalt-oxide. The presence of a certain fraction of cobalt oxide species that are more difficult to reduce can be due to the relatively strong cobalt-titania interactions as will be discussed below [41]. Despite these differences, the spectral parameters of the metallic contribution following reduction are the same for all samples, which confirms that the cobalt loading on titania cannot be used to obtain metallic cobalt particles of different size upon reduction at 340 °C. This is in line with the nearly similar sizes of the metallic cobalt particles as determined by TEM analysis (Fig. 1).

3.2. In situ Mössbauer emission spectroscopy during the FTS reaction

In situ Mössbauer spectra were recorded as a function of the steam partial pressure at a temperature of 200 °C, a total pressure of 20 bar, and a H_2/CO ratio of 4. The steam content in the feed is

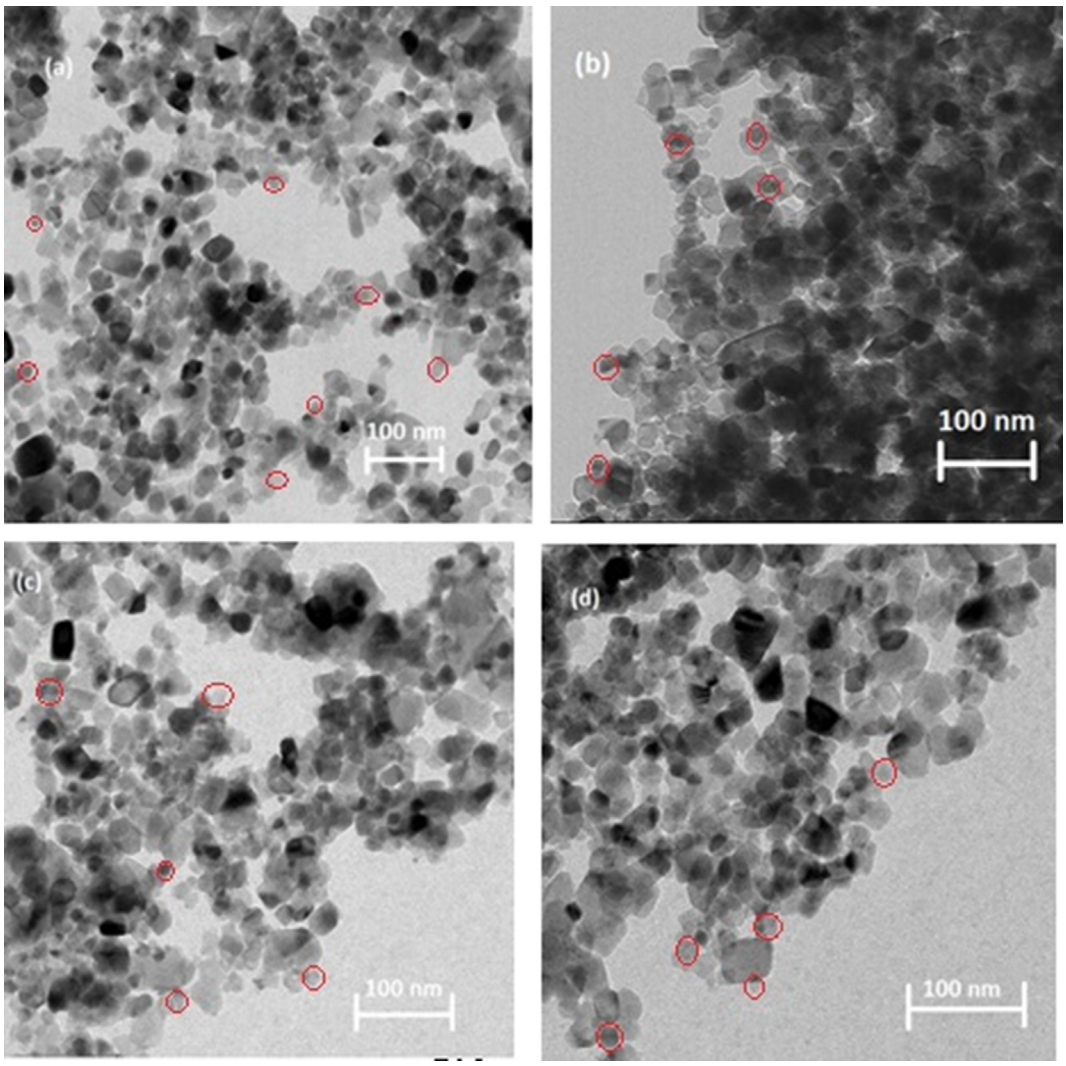

Fig. 1. Representative TEM images of (a) Co(2)/TiO_2, (b) Co(4) /TiO_2, (c) Co(6)/TiO_2 and (d) Co(8)/TiO_2 following reduction at 340 °C for 2 h and passivation in 5 % O_2 in He at room temperature. A few particles have been highlighted to assist the viewer.

expressed as the relative humidity (RH) at the applied conditions. Table S1 details the feed compositions for the different RH measurements. The actual RH during the Mössbauer measurements are slightly higher, as additional steam is produced by the FTS reaction. However, in a typical experiment with a CO conversion of approximately 15 %, the amount of produced steam is small compared to the amount of steam in the feed. When no steam is added, the RH due to the FTS reaction is ca. 1.5 %, which is substantially lower than the RH of 7.5 % of the first humidity step. Spectra were recorded for at least 48 h at each humidity step, except for RHs of 25 % and 57 % where the steam treatment was prolonged to 5 days and 11 days, respectively. This was done to understand the influence of prolonged exposure as encountered in industrial practice. We started by measuring MES spectra at 200 °C without steam added. The results in Table S3-S6 show that the cobalt distribution is very similar to the distribution obtained during room-temperature measurements after reduction in H_2.

When exposed to a relatively low partial pressure of steam (RH 7.5 %), the spectra of all catalysts contain the same metallic and oxidic features as observed directly after reduction (Fig. 4a). The predominant sextuplet has an IS of −0.2 mm s^{-1} and a HF of ∼ 310 kOe as measured at 200 °C and is independent of the cobalt loading, implying that the samples still contain magnetically ordered metallic cobalt particles. The oxidic doublet has an IS of 0.8 mm s^{-1} and a QS of 1.8 mm s^{-1}. The parameters point to a high dispersion of the Co^{2+}-oxide species, the large quadrupole splitting reflecting the low coordination of the cobalt atoms. While the contribution of this doublet is the same as under dry FTS conditions for Co(6)/TiO_2 and Co(8)/TiO_2, the contribution has increased for Co (2)/TiO_2 (from 23 % to 33 %) and Co(4)/TiO_2 (from 5 % to 13 %), pointing to cobalt oxidation. As the spectra do not show a significant change in the HF field for the metallic particles, these findings are likely not due to preferential oxidation of large or small particles, which would shift the average magnetic field to lower or higher values, respectively. Moreover, we can exclude a mechanism where only the surface of the metal particles is oxidized, as the fraction of oxidic cobalt formed in the Co(2)/TiO_2 and Co(4)/TiO_2 catalysts (10 % and 8 % respectively) exceeds the contribution of surface cobalt at the dispersion determined by TEM ($d_{average}$ 13 nm, dispersion 6 %). This will be further supported by the catalytic activity measurements presented below. Taken together, these results suggest mobility of cobalt species under the given conditions, leading to the formation of oxidized cobalt species in close interaction with the support as schematically shown in Fig. 5.

When the humidity is increased to RH values of 14 % and 20 %, further oxidation is observed. The spectral contribution of the oxi-

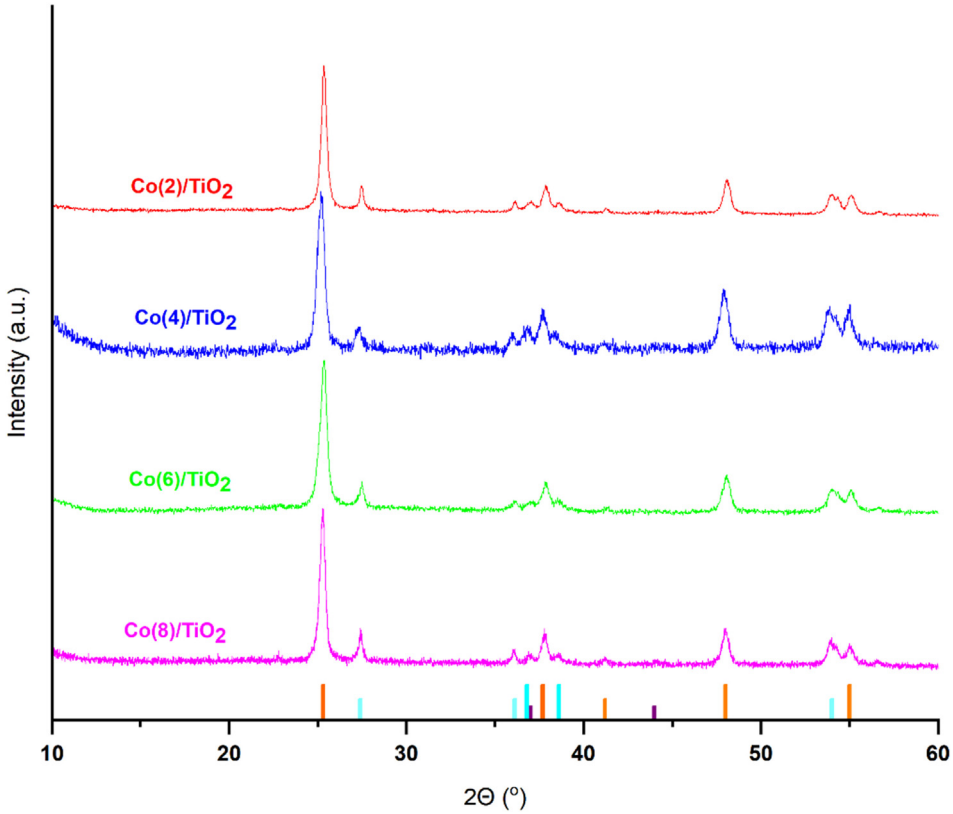

Fig. 2. X-ray diffractograms of Co(2)/TiO_2, Co(4)/TiO_2, Co(6)/TiO_2, and Co(8)/TiO_2 after calcination at 350 °C. The strongest diffraction lines of anatase TiO_2(orange), rutile TiO_2 (cyan) and Co_3O_4 (dark purple) are indicated at the bottom. (For interpretation of the references to colour in this figure legend, the reader is referred to the web version of this article.)

dic cobalt phase is given in Table 2 for all catalysts, while the Mössbauer fit parameters can be found in Tables S3-S6. Unfortunately, the spectral contribution for the Co(4)/TiO_2 catalyst after 48 h at RH 25 % and 57 % are not available due to a malfunction of the hardware during the long-term measurements. The spectra obtained at a relative humidity of 25 % are shown in Fig. 4b. At this RH, the Co(2)/TiO_2 sample contains an additional cobalt oxide state with an IS of 0.4 mm s^{-1} and a QS of 0.2 mm s^{-1}. The parameters can be assigned to Co^{3+}. The observation of Co^{3+} is most likely an artifact of the Mössbauer effect for ^{57}Co, where Co^{3+} is formed during the Auger cascade following the decay of the ^{57}Co probe [42–45]. Such a Co^{3+} signal is even present in the Mössbauer emission spectrum of ^{57}Co-doped CoO, which only contains Co^{2+} [42]. Surrounding Co^{2+} atoms can stabilize the Co^{3+} state, which is formed during the Auger cascade, long enough to be measured. As ^{57}Co probe atoms with more direct Co^{2+} neighbours are more likely to show this stabilized Co^{3+} state, the observation of Co^{3+} species by MES can be used as a qualitative indication for the dispersion of oxidic cobalt [46–48]. Thus, the data suggests that a larger amount of oxidic cobalt in the Co(2)/TiO_2 catalyst was present as slightly aggregated cobalt oxide than in the other catalysts at RH 25 %. Nevertheless, such a contribution becomes visible for the samples containing more cobalt upon increasing the humidity to 57 % (Fig. 4c). These findings indicate that, at elevated steam pressure, the amount of oxidic cobalt increases and the domain size of these oxidic structures becomes larger as schematically shown in Fig. 5. Since the measured HF of the metallic cobalt did not change, it is unlikely that higher humidity leads to oxidation of the larger metallic cobalt particles. Such a mechanism would have resulted in a change of the HF, because the HF is an average of the HFs of the metallic particles with different sizes. As such, we can conclude that the increasing amount of oxidic cobalt formed at higher humidity results in the growth of a cobalt oxide phase. It is likely that this phase is still highly dispersed as initially the Co^{3+} after-effect was absent.

Despite the similar initial cobalt particle size in the reduced samples, the evolution of cobalt oxide following exposure to steam under FTS conditions is seemingly different. Fig. 6 shows the absolute amount of oxidic cobalt formed as a function of the RH for the various samples. Within the experimental error, the samples contain a comparable amount of oxidic cobalt, which indicates that the extent of oxidation does not depend on the cobalt loading. The amount of oxidic cobalt increases with the steam pressure. Already at a low oxidizing potential (H_2O/H_2 0.25, RH 7.5 %), significant oxidation of metallic cobalt is observed for all prepared catalysts compared to the small contributions of cobalt oxide after reduction. The amount of oxidic cobalt increases to approximately 1.2 wt% cobalt under the harshest applied conditions (RH 57 %). We tentatively propose that this is due to the interaction of Co^{2+} with support hydroxyl groups, *i.e.*, titanol groups. P25 titania contains about 5 titanol groups per nm^2 [49]. Assuming a Co^{2+}:titanol stoichiometry of 2, the complete coverage of such surface groups would result in a cobalt loading of 1.2 wt%. The data can thus be interpreted in terms of oxidation of cobalt species under humid FTS conditions and their migration to stable locations at the support. When more cobalt is oxidized, these species might lead to highly dispersed cobalt oxide particles as suggested by the observation of a Co^{3+} signal. Nevertheless, we should also mention that there might be a role of the exposed anatase and rutile surfaces of titania with the P25 titania containing about 15 % rutile [40]. In the past, the impact of different titania phases on cobalt sintering and the formation of metal-support compounds has been suggested

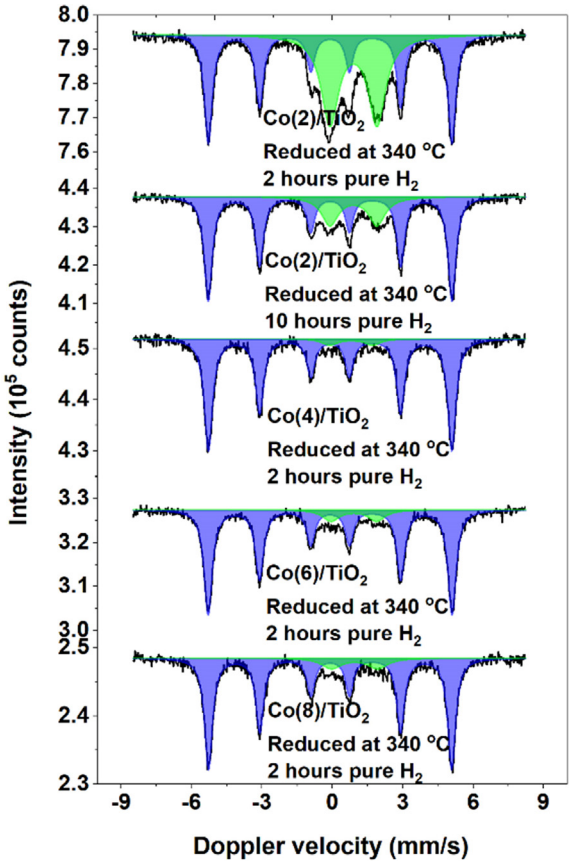

Fig. 3. Mössbauer spectra of reduced Co/TiO_2 catalysts at 340 °C in pure hydrogen: black lines represent the experimental spectra, blue the fitted bulk metallic cobalt and green the fitted cobalt oxide doublet. (For interpretation of the references to colour in this figure legend, the reader is referred to the web version of this article.)

[50–52]. The important corollary of these findings is that oxidation of cobalt is a possible pathway in the deactivation of titania-supported cobalt nanoparticle catalysts during the FTS reaction. Thermodynamic considerations showed that cobalt oxidation under FTS conditions is not favorable for cobalt metal particles larger than 4 nm [11]. The present results show that oxidation of cobalt can occur under industrially relevant conditions for cobalt particles larger than 6 nm. The observed oxidation does not involve oxidation of metallic cobalt particles and, following the discussion above, also not from oxidation of a surface layer of the metallic cobalt nanoparticles as found for cobalt on silica [53]. Kliewer et al. mentioned that oxidation of cobalt on titania results in cobalt oxide/hydroxide species that anchor to the titania support [29]. Based on the latter suggestions and the current findings, we propose that the mobility of metallic cobalt species in combination with the oxidizing conditions due to water play a role in oxidizing cobalt forming dispersed cobalt oxide interacting with titanol groups as sketched in Fig. 5. Thus, whilst bulk oxidation did not occur under humid FTS conditions in line with the conclusions of Van Steen et al. [11], our findings show that dispersed oxidic cobalt can be formed in titania-supported cobalt catalysts under realistic FTS conditions. It is likely that the strong cobalt-titania support interactions play a critical role here, as oxidation was not observed for cobalt nanoparticles supported on carbon nanofibers treated under similar reaction conditions [35]. Beck et al. [54,55] found that metallic platinum particles enhance the formation of oxygen vacancies in titania at a relatively low reduction temperature. Although we did not study the reduction of the titania surface for our catalysts, we argue that, even if oxygen vacancies would have formed under reducing conditions, these would be hydroxylated in the presence of steam. For instance, an STM study reported that H_2O dissociates on oxygen vacancies of titania already at 120 K by donating a proton to an adjacent oxygen and forming a bridged hydroxyl group [56–58]. The reducibility of small oxidic cobalt particles in synthesis gas can be affected by the presence of oxygen vacancies. Recent work by Qiu et al. indicated that oxygen vacancies in the titania support material enhance the reducibility of especially relatively small cobalt oxide particles [59]. Thus, the presence of steam, which keeps the surface in an oxidized/hydroxylated state, might inhibit reduction of the small cobalt oxide particles. The work by Kliewer et al. [29] reported that the presence of oxidic cobalt on titania can enhance the sintering of the active phase. If significant sintering of metallic cobalt occurred under humid FTS, an increase of the HF parameter would be observed. However, this parameter remains constant throughout the humid treatments for all catalyst samples (Tables S3-S6). Upon reduction of the oxidic cobalt formed during FTS, an increased metallic cobalt content is observed for all catalyst samples. This increased degree of reduction indicates growth of the oxidic cobalt domains, as small oxidic particles are typically more difficult to reduce [15]. This is in good agreement with the observation of after-effect Co^{3+} species, as its observation can be attributed to larger oxidic agglomerates. So, whilst no increase in the measured HF is observed between the freshly reduced and spent reduced state (Tables S3-S6), the improved reducibility points towards the agglomeration of oxidic cobalt during humid FTS. We also considered the alternative deactivation pathway under simulated high CO conversion conditions through formation of metal-support compounds [52,60]. Such studies have shown before that cobalt titanate readily forms at high humidity, especially for a pure anatase titania support. We did not even observe cobalt titanate species under our harshest humid FTS conditions of RH 57 %. Compared to literature where a H_2O/H_2 ratio of 70 was used in the absence of CO, our highest H_2O/H_2 ratio of 1 can nevertheless explain this difference.

3.2.1. Sintering under humid Fischer-Tropsch conditions

Our findings indicate that the active cobalt phase in titania-supported FTS catalysts can sinter upon partial oxidation under humid FTS conditions and subsequent reduction. Under the given measurement conditions, the HF parameter does not allow picking up such sintering of the metallic cobalt nanoparticles. Our previous work on carbon-supported cobalt, however, showed very clearly enhanced sintering of cobalt nanoparticles upon steam treatment in the presence of CO [34]. Accordingly, we studied the sintering of cobalt on titania in more detail by reducing $Co(2)/TiO_2$ at a lower temperature of 300 °C in order to obtain initially smaller metallic cobalt particles. The resulting MES spectra are given in Fig. 7 and the corresponding Mössbauer parameters are listed in Table S7. Compared to reduction at 340 °C, the spectra contain a much larger contribution of oxidic cobalt, both in the form of Co^{2+} (36 %) and Co^{3+} (39 %) next to a metallic cobalt contribution of 25 %, characterized by the usual sextuplet for larger than 6 nm cobalt nanoparticles. To study sintering, we recorded MES spectra at a higher temperature of 200 °C. The higher measurement temperature can result in the loss of magnetic ordering for relatively small cobalt nanoparticles. This is evident from the spectra recorded at 200 °C (Fig. 7) after heating in a flow of inert argon, where the metallic cobalt phase is now characterized by a singlet with an IS of 0.0 mm s^{-1}, in addition to the sextuplet representative of bulk metallic cobalt particles. The loss of magnetic ordering of a fraction of the cobalt nanoparticles at a higher measurement temperature implies that their size is smaller than 6 nm [34]. We refer to these particles as superparamagnetic (SPM) cobalt. The contribution of SPM cobalt is 29 %, while the contribution of bulk cobalt is 16 %.

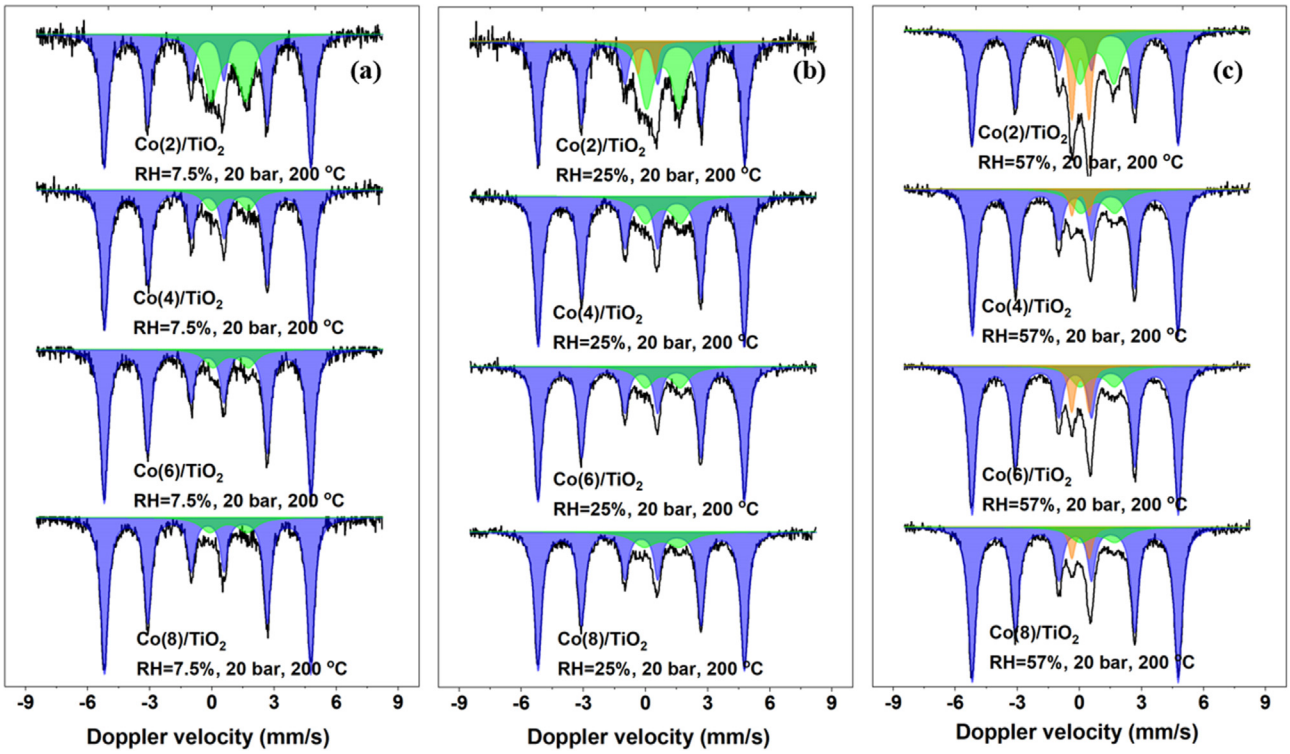

Fig. 4. (a) *In situ* Mössbauer spectra of the Co/TiO_2 catalysts under FTS conditions at a relative humidity of (a) 7.5%, (b) 25% and (c) 57%. The black lines represent the experimental spectra, the blue ones the fitted metallic cobalt sextuplet and the orange and green ones the fitted cobalt oxide doublets. (For interpretation of the references to colour in this figure legend, the reader is referred to the web version of this article.)

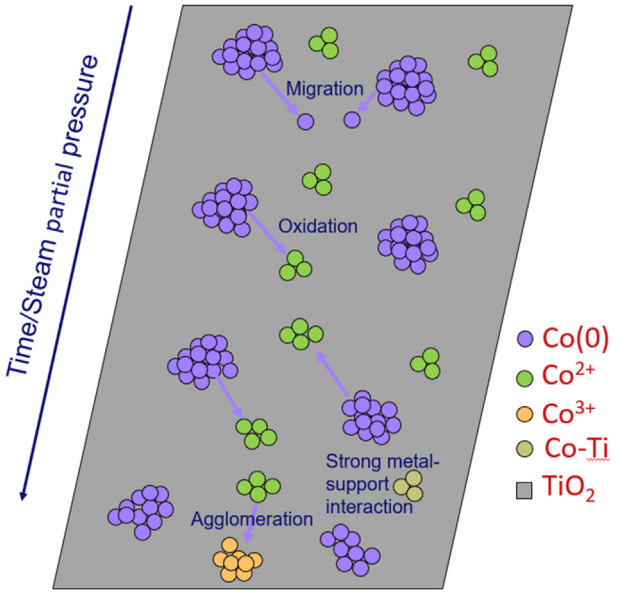

Fig. 5. Schematic representation of the different cobalt species present in the catalyst and their evolution during the FTS reaction under changing conditions.

The combined spectral contribution of bulk and SPM cobalt is 45 %, which is significantly larger than the metallic contribution of 25 % derived from spectra recorded at room temperature. When measuring at elevated temperatures, difference in the Debye temperature of the different phases can lead to over- or underestimation of the spectral contributions [61]. Accordingly, we explain the difference in spectral contribution between the room-temperature and 200 °C measurements under inert conditions to the higher Debye temperatures of the metallic phases in comparison with the oxidic cobalt phases. Additionally, the contribution from Co^{3+} declined significantly from 39 % to 14 %, whilst the Co^{2+} contribution increased from 36 % to 41 %. This suggests that the above-discussed Mössbauer after-effects are less pronounced at elevated temperatures. Nevertheless, despite the differences between room-temperature and 200 °C measurements, the Mössbauer data at the higher temperature can still be used for a qualitative analysis of sintering as will be done in the following.

Upon introduction of dry synthesis gas, the SPM cobalt feature in the spectrum recorded at 200 °C remains with an IS of -0.1 mm s^{-1} and a spectral contribution of 26 %. Under these conditions, the Co^{3+} doublet is no longer present, and the spectral contribution of the Co^{2+} doublet has increased from 41 % to 45 %. The combined spectral contribution of oxidic cobalt thus decreased from 55 % to 45 % whilst the temperature remained the same, indicating some reduction occurs under these conditions, likely of the largest oxidic cobalt species. The remaining spectral contribution of 29 % is made up by relatively large, magnetically ordered metallic cobalt particles. Upon addition of steam to the feed, the SPM cobalt contribution is immediately lost, even at a low RH of 7.5 %. Under these slightly humid FTS conditions, the bulk metallic contribution increased from 29 % to 74 % with the residual 26 % corresponding to Co^{2+}. These results clearly show that the addition of steam to the synthesis gas feed leads to mobility of cobalt on the titania surface, resulting in further reduction of dispersed oxidic cobalt as well as sintering of small metallic particles. These findings support the previous hypothesis that carbon monoxide and steam have a synergistic effect towards sintering [21,34,35] and that this also occur on titania. Kliewer et al. [29] suggested that the presence of oxidic cobalt on the titania facilitates sintering of the metallic phase due to coalescence following reduction. The present findings support such a mechanism as both an increased reduction degree and particle growth are observed simultaneously.

Table 2
Contribution of cobalt oxide phase (Co^{2+} and Co^{3+} species) as determined from MES spectra recorded at 200 °C under varying FTS conditions.

Treatment	*H_2O/H_2*	*Treatment length (hrs)*	*Spectral contribution cobalt oxide (%)*			
			$Co(2)/TiO_2$	*$Co(4)/TiO_2$*	*$Co(6)/TiO_2$*	*$Co(8)/TiO_2$*
RH 0 %	0	48	23	5	9	8
RH 7.5 %	0.25	48	33	13	11	10
RH 14 %	0.50	48	34	14	12	11
RH 20 %	0.75	48	35	14	13	13
RH 25 %	1.0	48	36	N/A	14	13
	1.0	120	37	16	14	14
RH 57 %	1.0	48	37	N/A	17	16
	1.0	120	40	N/A	19	17
	1.0	264	43	20	22	17

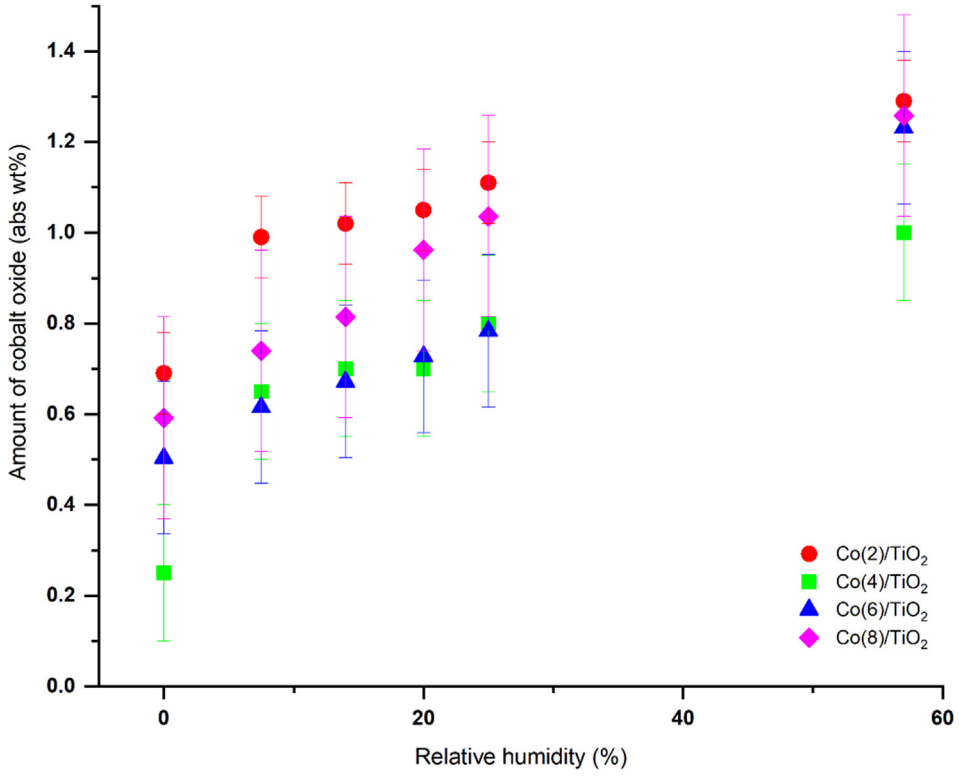

Fig. 6. Amount of cobalt oxide in Co/TiO_2 catalysts under humid Fischer-Tropsch conditions (200 °C, 20 bar, $H_2/CO = 4$) as determined by Mössbauer spectroscopy at 200 °C as a function of the relative humidity (red: $Co(2)/TiO_2$, green: $Co(4)/TiO_2$, blue: $Co(6)/TiO_2$, magenta: $Co(8)/TiO_2$). (For interpretation of the references to colour in this figure legend, the reader is referred to the web version of this article.)

The improved reduction is likely also facilitated by hydrogen spillover, which is facilitated by the presence of steam [62,63]. Overall, these phenomena can contribute to cobalt sintering and a higher cobalt reduction degree, despite the increasing oxidizing potential due to the higher steam pressure.

3.3. Characterization used catalysts

To complement the Mössbauer data obtained under humid FTS conditions, STEM-EDX measurements were performed on reduced-passivated and used $Co(4)/TiO_2$. The term 'used catalysts' refers to the non-radioactive catalyst samples obtained from the Mössbauer cell under the same humid FTS treatments as the Mössbauer samples. As such, these measurements provide *ex situ* information about the state of the catalyst following the deactivation studies. For each sample, 8 EDX maps were obtained on different areas of the sample. Two representative maps of the reduced and passivated $Co(4)/TiO_2$ are shown in Fig. 8a-b. These are broadly in keeping with the earlier bright-field TEM measurements discussed above, showing the presence of cobalt particles with sizes in the range of 10–16 nm dispersed over the titania support.

Representative maps of used $Co(4)/TiO_2$ following high humidity FTS conditions are given in Fig. 8c-d. The cobalt particles are larger than in the reduced-passivated sample with sizes in the 16–22 nm range. This is despite the fact that the HF of the metallic cobalt phase during humid FTS did not increase, highlighting again that this parameter is not sensitive enough to detect the sintering occurring under these conditions. This supports the earlier conclusion that steam addition to the synthesis gas feed leads to cobalt sintering. However, some small cobalt particles (5–8 nm) can still be observed in some of the STEM-EDX maps. These small particles may be due to the small amount of cobalt that was not reduced according to MES (Table S4), even after re-reduction following exposure to high humidity FTS conditions. Based on the particle size distribution shown in Table 1, this could correspond to relatively small cobalt particles with a size smaller than 8.5 nm.

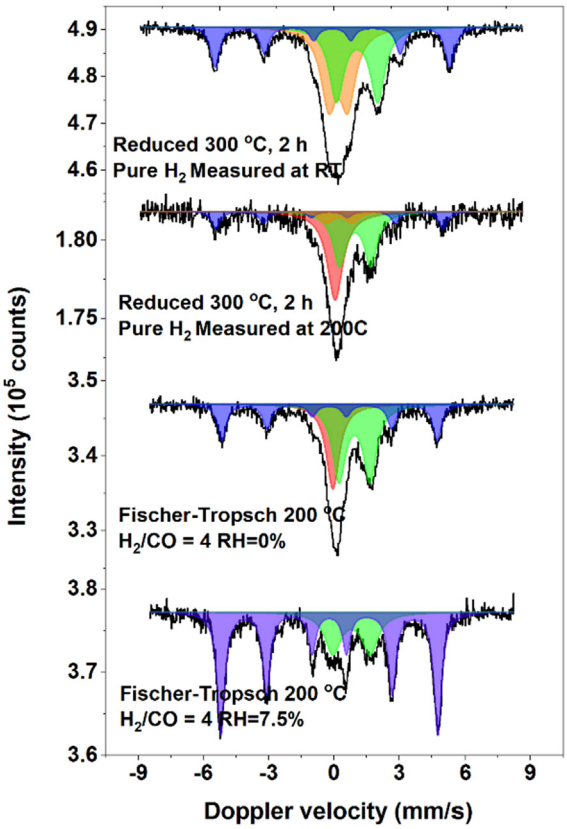

Fig. 7. *In situ* Mössbauer spectra measured of Co(2)/TiO_2 following reduction at 300 °C and exposure to different FTS conditions: black lines represent the experimental spectra, blue ones the fitted metallic bulk cobalt sextuplet, red ones the small metallic cobalt singlet, and the orange and green ones the fitted cobalt oxide doublets. (For interpretation of the references to colour in this figure legend, the reader is referred to the web version of this article.)

Regardless, this data shows that, besides the evident oxidation, sintering is also a significant deactivation pathway on titania-supported cobalt catalysts during humid FTS.

3.4. Oxidation in the absence of CO

To study the oxidation behaviour of Co/TiO_2 at higher oxidizing potential in the absence of CO, we subjected Co(4)/TiO_2 to model oxidation conditions (Fig. 9). This sample was selected, because it combines a relatively low cobalt loading with good cobalt reducibility. The Mössbauer spectra were measured *in situ* at 220 °C and 20 bar at a constant RH of 25 %, while varying the H_2O/H_2 ratio in the feed. The compositions used in these model oxidation measurements are given in Table S2. The Mössbauer parameters obtained during these experiments are collected in Table S8. Following 2 h reduction in pure hydrogen at 340 °C, a bulk metallic cobalt phase (83 %) was observed with an IS of −0.1 mm s^{-1} and a HF of 309 kOe measured at 220 °C. The residual spectral contribution belongs to dispersed Co^{2+}-oxide with an IS of 0.8 mm s^{-1} and a QS of 1.7 mm s^{-1}. The spectra obtained at a H_2O/H_2 ratio of 10 contains the same two cobalt features, but the spectral contribution of the bulk metallic cobalt was lower at 65 % with the other 35 % corresponding to the dispersed Co^{2+}-oxidic phase. Increasing the H_2O/H_2 ratio to 50 by reducing the H_2 partial pressure resulted in a further increase of the cobalt oxide content to 55 %. When the ratio was further increased to 70, a new cobalt oxide doublet was observed (55 %) with an IS of 0.5 mm s^{-1} and a QS of 1.2 mm s^{-1}, which corresponds to a second Co^{2+} feature distinctively different from the other Co^{2+} species. At such a high H_2O/H_2 ratio, the formation of cobalt titanates can be envisioned. In $CoTiO_3$, Co also has a formal 2 + oxidation state but a different coordination environment than in CoO. The Mössbauer parameters of this Co^{2+} phase are very similar to those reported for ferrous titanate ($FeTiO_3$) [64]. Thus, we infer that cobalt titanate phase was formed. When hydrogen is fully removed from the feed, full oxidation is observed with the cobalt-titanate feature, having a high spectral contribution of 76 % and dispersed cobalt oxide making up the remainder. Following these lengthy model oxidation treatments, the reduction of the fully oxidized catalyst was investigated. Notably, a degree of reduction of only 18 % was obtained following reduction at 340 °C for 2 h. The dominant Co^{2+} feature could only be removed by reduction at 450 °C, further strengthening the hypothesis that this doublet corresponded to cobalt titanate [65]. Contrary to the previous humid FTS measurements, no Co^{3+} features were observed during model oxidation. These findings suggest that, in the absence of CO, the agglomeration of the oxidic cobalt domains is significantly less pronounced. The slight gradual decrease of the HF from 309 kOe in the reduced state to 307 kOe at the highest H_2O/H_2 ratio of 70 also indicates that the metallic particles are becoming smaller, as the measured HF follows from the average particle size. This either suggests that larger metallic particles are oxidized before smaller ones or that gradual oxidation of the surface of cobalt particles occurs. Both mechanisms can explain the observed drop in HF. Contrary to humid FTS conditions, under the highly oxidizing conditions in these measurements the oxidic cobalt species react with the titania support to form metal-support compounds as previously reported by Wolf et al. [52]. This is also shown schematically in Fig. 5. So, although the inclusion of cobalt in $CoTiO_3$-like surface compounds would represent a significant deactivation pathway, these compounds are only formed under unusual conditions of very high H_2O/H_2 ratio (>70), which are less relevant to practical FTS.

3.5. Deactivation pathways on the titania support

Based on the present findings we sketched a deactivation mechanism for Co/TiO_2 in Fig. 10. We propose that, under low oxidizing potential (RH = 7.5–20 %, H_2O/H_2 < 1), the presence of steam during FTS conditions results in sintering of small metallic particles as well as the formation of dispersed oxidic cobalt on the titania support. The formation of oxidic cobalt complexes with the titania support has been earlier observed following deposition of cobalt on titania in aqueous media [66]. Whilst we cannot determine the exact nature of the oxidic cobalt observed in this work, it is very likely that such structures are formed. The cobalt oxidation degree increases with at higher oxidizing potential of the reaction mixture. Depending on the presence of carbon monoxide, different deactivation pathways are followed. With carbon monoxide present, it is likely that mobile cobalt carbonyl species contribute to further growth of the oxidic cobalt species into larger domains and facilitate sintering of the metallic cobalt via Ostwald ripening as has been previously observed [7]. A density functional theory study showed that the formation of cobalt carbonyl species is energetically favourable under practical FTS conditions, even in the presence of adsorbed water [67]. The loss of metallic cobalt lowers the FTS activity, while re-reduction can result in the loss of the metallic cobalt surface area due to sintering through coalescence. Due to the relatively low oxidizing potential (H_2O/H_2 = 1) under our humid FTS conditions, no formation of cobalt-titanate compounds is observed. However, without CO, the mobility of cobalt seems hampered, as no larger oxidic cobalt domains are observed

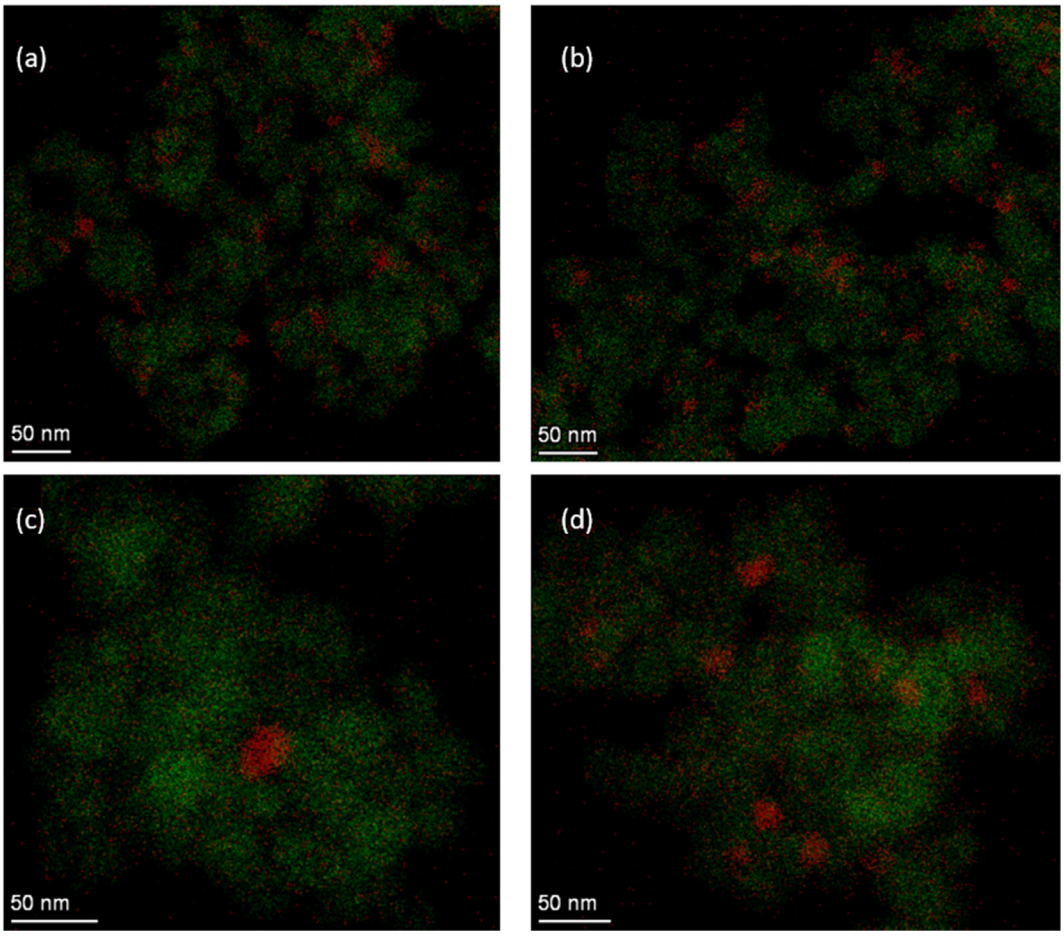

Fig. 8. EDX mappings of (a-b) a reduced and passivated and (c-d) a used Co(4)/TiO_2 catalyst: the cobalt mapping is shown in red and the titania mapping in dark green. (For interpretation of the references to colour in this figure legend, the reader is referred to the web version of this article.)

in the form of Co^{3+} despite the high degree of oxidation. When the oxidizing potential is significantly increased (H_2O/H_2 = 70) the formation of $CoTiO_3$-like structures is observed, formed by the strong interaction of the dispersed oxidic cobalt with the titania support. Reduction of these structures requires much higher temperatures, meaning that a larger amount of cobalt is no longer accessible for catalysis.

3.6. Catalytic performance

The catalytic activity continuously measured on-stream during the Mössbauer measurements is given in Fig. 11. The results of the sample with the lowest cobalt loading (Co(2)/TiO_2) are not shown, as the conversion was too low. The other catalysts show very similar activity trends in terms of a slow decrease of the CO conversion with increasing humidity. It is important to note that the opposite has also been reported, namely that water co-feeding can increase FTS activity [68,69]. Additionally, the introduction of steam to the reactor feed results in a small decrease of the CO and H_2 partial pressures, which can affect the catalytic activity due to the negative reaction order in CO and positive order in H_2 [70,71]. Therefore, additional measurements were performed under dry conditions following the 5-day treatment at RH = 25 %. This did not lead to significant activity differences. As such, the observed deactivation can be linked to the gradual oxidation of the active metallic cobalt along with mild sintering, resulting in a decrease of the cobalt specific activity of approximately 20 % for all catalysts when comparing dry and RH 57 % conditions. This activity loss exceeds the loss of metallic cobalt between dry and high humidity conditions for all catalysts, indicating that oxidation of metallic cobalt can only explain part of the deactivation. It underlines that sintering, as observed by STEM-EDX (Fig. 10), also significantly contributes to deactivation. Full surface oxidation of metallic cobalt particles can be excluded as a mechanism, as the formation of a (thin) surface oxide layer on metallic cobalt particles would render the active catalytic sites completely inaccessible for catalysis, resulting in a far greater activity loss already at relatively low oxidizing potential (RH = 7.5 %).

Besides catalytic activity measurements in the *in situ* MES cell, the performance of the cobalt catalysts was measured in a high-pressure fixed-bed plug-flow reactor at 220 °C, 20 bar, a H_2/CO ratio of 4, and a space velocity of 60 L $g_{cat}^{-1}h^{-1}$. The corresponding results for fresh and used catalysts are collected in Table 3. Note that the fresh catalysts were reduced at 340 °C for 2 h, while the used catalysts retrieved after the *in situ* MES measurements were re-reduced according to the same procedure. The activity normalized on the amount of cobalt (CTY) was in the range of 1.7–2.2 10^{-5} $mol_{CO}\ g_{Co}^{-1}\ s^{-1}$ for the fresh reduced catalysts. The Co(2)/TiO_2 catalyst shows a substantially higher CTY after exposure to humid Fischer-Tropsch conditions. This strong increase is likely the result of the higher cobalt reduction degree, following the harsh humid FTS conditions employed. We previously showed that 47 % of cobalt remained oxidic when the fresh catalyst was reduced for 2 h at 340 °C, whereas only 18 % remained oxidic after 2 h at the

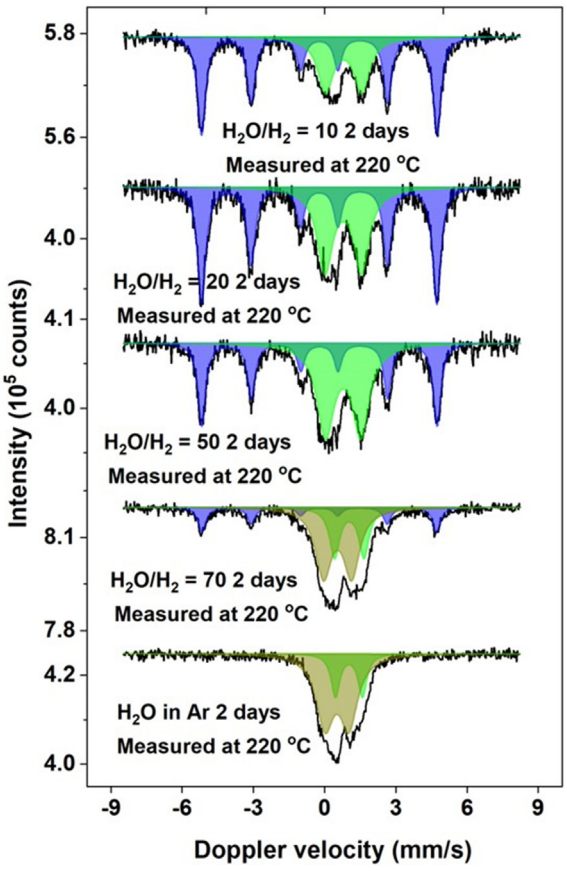

Fig. 9. *In situ* Mössbauer spectra measured of Co(4)/TiO_2 following model oxidation treatments: black lines represent the experimental spectra, blue ones the fitted metallic bulk cobalt sextuplet, and dark yellow and green ones the fitted cobalt oxide doublets. (For interpretation of the references to colour in this figure legend, the reader is referred to the web version of this article.)

same reduction temperature for the used catalyst. As the catalysts for these activity measurements were reduced *in situ* for 2 h, one would expect significant differences in the amount of metallic cobalt and, thus, the catalytic performance. This higher degree of reduction for the used catalysts counteracts the negative impact of sintering on the activity. In good agreement with this, the CTY of the used Co(2)/TiO_2 catalyst is approximately 50 % higher than that of the fresh catalyst. The relatively strong increase in activity suggests that deactivation due to sintering was minimal. However, the used catalyst shows a significantly larger contribution of C5 + hydrocarbon products at the expense of methane. It has been previously shown that an increase in the cobalt particle size results in an increased C5 + selectivity under high pressure FTS conditions [4], although this effect becomes much less pronounced for cobalt particles larger than 10 nm. Therefore, this change in selectivity can be in part explained by sintering of metallic particles. The increase in CO conversion likely leads to an increased selectivity towards C5 + products. The used Co(4)/TiO_2 catalyst is less active than the fresh one, as expected since the STEM-EDX maps clearly show significant sintering of the cobalt particles. In this case, there was no benefit for the increased reducibility of the used catalyst compared to its fresh state. However, contrary to the Co(2)/TiO_2 catalyst, the used Co(4)/TiO_2 catalyst shows a higher selectivity towards methane compared to the fresh one. This shift in selectivity could be the result of the lower CO conversion, as lower CO conversion typically shifts the selectivity towards C1 products due to the lower coverage of the surface with chain-growth monomers. The two catalysts with the highest weight loadings show almost identical CTY values, which are comparable to what was observed for the fresh Co(4)/TiO_2 catalyst. This underlines the structural similarity between these catalysts with the comparable particle sizes resulting in similar catalytic performance. The two fresh catalysts exhibit a similar selectivity towards C5 + hydrocarbons, but lower than for the Co(4)/TiO_2 catalyst, despite the higher CO conversion. Nevertheless, the observed changes are relatively small and the obtained product distributions are typical for the FTS reaction under our hydrogen-rich conditions.

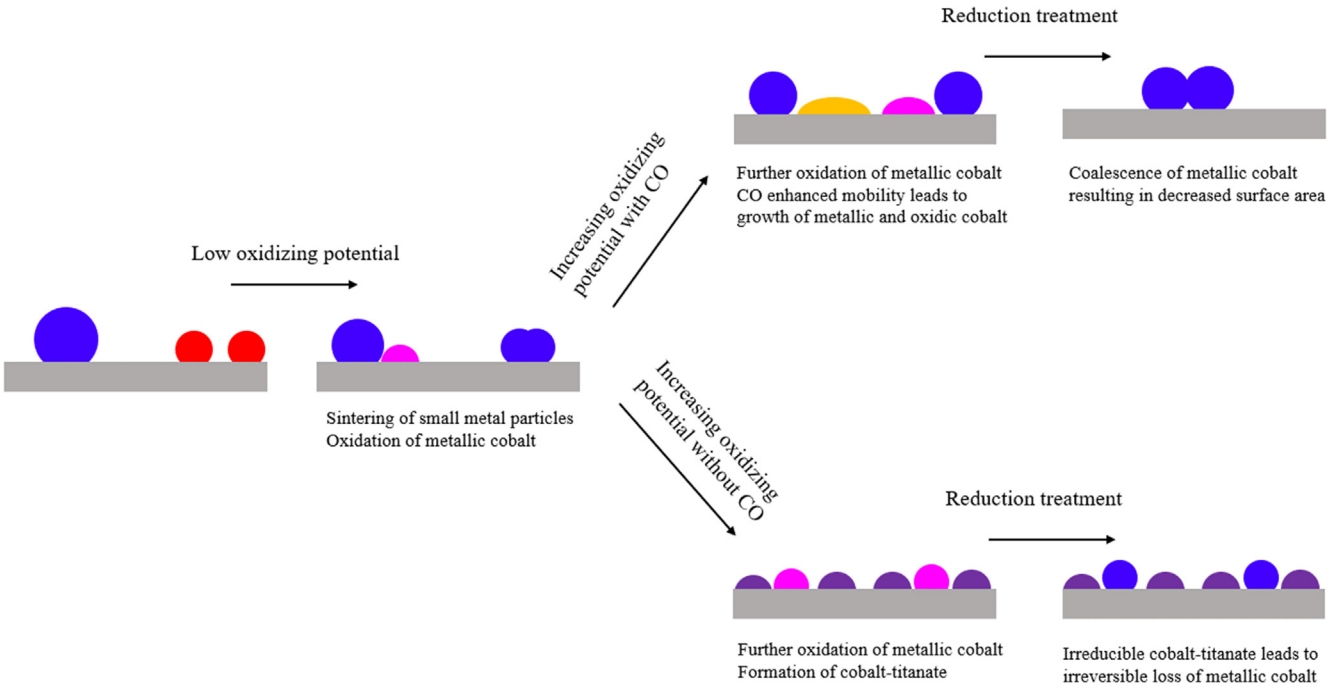

Fig. 10. Schematic representation of deactivation mechanisms observed for Co/TiO2 catalysts. Shown are small metallic SPM cobalt (red), bulk metallic cobalt (dark blue), dispersed oxidic cobalt (magenta), aggregated oxidic cobalt (orange), cobalt-titanate (dark purple), and titania (grey). (For interpretation of the references to colour in this figure legend, the reader is referred to the web version of this article.)

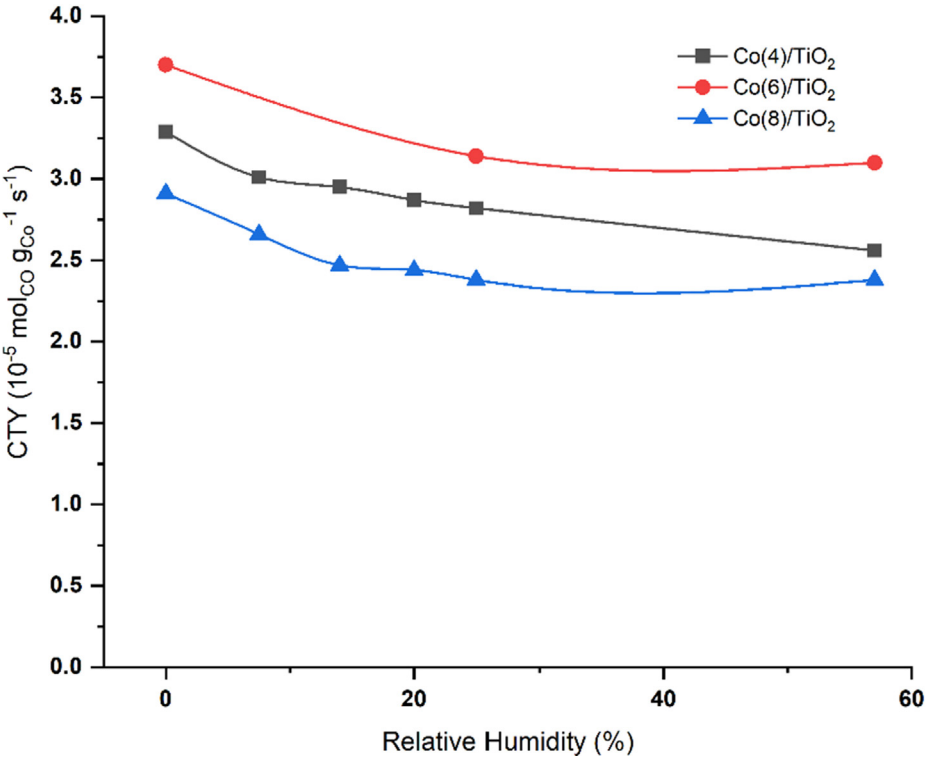

Fig. 11. *In situ* FTS activity of the Co(x)/TiO_2 catalysts during humid FTS measurements in the Mössbauer cell. The CTY determined at steady state at the applied conditions is plotted against the RH. (Co(4)/TiO_2: black squares, Co(6)/TiO_2: red circles, Co(8)/TiO_2: blue triangles). (For interpretation of the references to colour in this figure legend, the reader is referred to the web version of this article.)

Table 3
Catalytic performance data for the cobalt catalysts (plug-flow reactor operated at 220 °C, 20 bar and H_2/CO = 4, SV = 60 L $g_{cat}^{-1}h^{-1}$).

Catalyst	*Conversion (%)*	*C_1 selectivity (%)*	*C_2-C_4 selectivity (%)*	*C_{5+} selectivity (%)*	*CTY (10^{-5} mol_{CO} g_{Co}^{-1} s^{-1})*
Co(2)/TiO_2	2	12	7	81	1.6
Co(2)/TiO_2 used	4	5	3	92	2.5
Co(4)/TiO_2	3	7	7	86	2.1
Co(4)/TiO_2 used	1	14	10	76	1.2
Co(6)/TiO_2	5	11	9	80	1.9
Co(8)/TiO_2	5	15	9	76	1.9

4. Conclusion

By combining Mössbauer spectroscopy with TEM, we showed that reduction of a calcined cobalt on titania precursor led to sintering. Independent of the initial cobalt loading in the 2–8 wt% range, the final size of the reduced cobalt metal particles was the same (ca. 12 nm). *In situ* Mössbauer spectroscopy demonstrated partial oxidation of metallic cobalt under humid FTS conditions. The extent of cobalt oxidation increased with the steam partial pressure. Comparing the different catalysts, it was found that the absolute amount of oxidized cobalt was the same for all samples. This could be linked to cobalt oxide strongly interacting with titanol groups of the support. The formation of cobalt-titanate-like compounds was only observed under very high oxidizing potential and in the absence of CO. As such, our results indicate that such compounds do not readily form under practical FTS conditions. The data point to a strong impact of humid FTS conditions on the sintering of small metallic cobalt particles, where oxidic cobalt wets the titania support, facilitating cobalt sintering in synthesis gas and under reduction conditions. STEM-EDX maps confirmed the much larger cobalt particles in catalysts employed under humid FTS conditions in comparison to reduced samples.

Data availability

Data will be made available on request.

Declaration of Competing Interest

The authors declare that they have no known competing financial interests or personal relationships that could have appeared to influence the work reported in this paper.

Acknowledgements

Luke van Koppen acknowledges the financial support from Shell Global Solutions International B.V.. The authors thank Dr. Mengyue Wu from Kavli Institute at TU Delft for assistance with STEM-EDX experiments.

Appendix A. Supplementary material

Experimental conditions, Mössbauer fit parameters.

Supplementary data to this article can be found online at https://doi.org/10.1016/j.jcat.2023.02.019.

References

[1] E. Iglesia, Design, synthesis, and use of cobalt-based Fischer-Tropsch synthesis catalysts, Appl. Catal. A Gen. 161 (1–2) (1997) 59–78, https://doi.org/10.1016/S0926-860X(97)00186-5.

[2] E. Rytter, N.E. Tsakoumis, A. Holmen, On the selectivity to higher hydrocarbons in Co-based Fischer-Tropsch synthesis, Catal. Today 261 (2016) 3–16, https://doi.org/10.1016/j.cattod.2015.09.020.

[3] J.P. den Breejen, P.B. Radstake, G.L. Bezemer, J.H. Bitter, V. Frøseth, A. Holmen, K.P. de Jong, On the Origin of the Cobalt Particle Size Effects in Fischer–Tropsch Catalysis, J. Am. Chem. Soc. 131 (20) (May 2009) 7197–7203, https://doi.org/10.1021/ja901006x.

[4] G.L. Bezemer, J.H. Bitter, H.P.C.E. Kuipers, H. Oosterbeek, J.E. Holewijn, X. Xu, F. Kapteijn, A.J. van Dillen, K.P. de Jong, Cobalt Particle Size Effects in the Fischer–Tropsch Reaction Studied with Carbon Nanofiber Supported Catalysts, J. Am. Chem. Soc. 128 (12) (Mar. 2006) 3956–3964, https://doi.org/10.1021/ja058282w.

[5] N.E. Tsakoumis, M. Rønning, Ø. Borg, E. Rytter, A. Holmen, Deactivation of cobalt based Fischer-Tropsch catalysts: A review, Catal. Today 154 (3–4) (2010) 162–182, https://doi.org/10.1016/j.cattod.2010.02.077.

[6] P.J. van Berge, R.C. Everson, Cobalt as an alternative Fischer-Tropsch catalyst to iron for the production of middle distillates, Stud. Surface Sci. Catal. 107 (15) (1997) 207–212, https://doi.org/10.1016/S0167-2991(97)80336-9.

[7] D. Moodley, M. Claeys, E. van Steen, P. van Helden, D. Kistamurthy, K.-J. Weststrate, H. Niemantsverdriet, A. Saib, W. Erasmus, J. van de Loosdrecht, Sintering of cobalt during FTS: Insights from industrial and model systems, Catal. Today 342 (Feb. 2020) 59–70, https://doi.org/10.1016/j.cattod.2019.03.059.

[8] E. Rytter, A. Holmen, Deactivation and regeneration of commercial type fischer-tropsch co-catalysts—A mini-review, Catalysts 5 (2) (2015) 478–499, https://doi.org/10.3390/catal5020478.

[9] Z. Yu, Ø. Borg, D. Chen, E. Rytter, A. Holmen, Role of surface oxygen in the preparation and deactivation of carbon nanofiber supported cobalt Fischer-Tropsch catalysts, Top. Catal. 45 (1–4) (Aug. 2007) 69–74, https://doi.org/10.1007/s11244-007-0242-7.

[10] M. Wolf, B.K. Mutuma, N.J. Coville, N. Fischer, M. Claeys, Role of CO in the Water-Induced Formation of Cobalt Oxide in a High Conversion Fischer-Tropsch Environment, ACS Catal. 8 (5) (May 2018) 3985–3989, https://doi.org/10.1021/acscatal.7b04177.

[11] E. Van Steen, M. Claeys, M.E. Dry, J. Van De Loosdrecht, E.L. Viljoen, J.L. Visagie, Stability of nanocrystals: Thermodynamic analysis of oxidation and re-reduction of cobalt in water/hydrogen mixtures, J. Phys. Chem. B 109 (8) (2005) 3575–3577, https://doi.org/10.1021/jp045136o.

[12] P.J. Van Berge, J. Van De Loosdrecht, S. Barradas, A.M. Van Der Kraan, Oxidation of cobalt based Fischer-Tropsch catalysts as a deactivation mechanism, Catal. Today 58 (4) (2000) 321–334, https://doi.org/10.1016/S0920-5861(00)00265-0.

[13] J. van de Loosdrecht, B. Balzhinimaev, J.A. Dalmon, J.W. Niemantsverdriet, S.V. Tsybulya, A.M. Saib, P.J. van Berge, J.L. Visagie, Cobalt Fischer-Tropsch synthesis: Deactivation by oxidation?, Catal Today 123 (1–4) (2007) 293–302, https://doi.org/10.1016/j.cattod.2007.02.032.

[14] W. Zhou, J.-G. Chen, K.-G. Fang, Y.-H. Sun, The deactivation of Co/SiO_2 catalyst for Fischer-Tropsch synthesis at different ratios of H_2 to CO, Fuel Process. Technol. 87 (7) (Jul. 2006) 609–616, https://doi.org/10.1016/j.fuproc.2006.01.008.

[15] G. Prieto, A. Martínez, P. Concepción, R. Moreno-Tost, Cobalt particle size effects in Fischer-Tropsch synthesis: structural and in situ spectroscopic characterisation on reverse micelle-synthesised Co/ITQ-2 model catalysts, J. Catal. 266 (1) (Aug. 2009) 129–144, https://doi.org/10.1016/j.jcat.2009.06.001.

[16] M. Wolf, E.K. Gibson, E.J. Olivier, J.H. Neethling, C.R.A. Catlow, N. Fischer, M. Claeys, In-depth characterisation of metal-support compounds in spent Co/SiO_2 Fischer-Tropsch model catalysts, Catal. Today 342 (Feb. 2020) 71–78, https://doi.org/10.1016/j.cattod.2019.01.065.

[17] C.H. Bartholomew, Mechanisms of catalyst deactivation, Appl. Catal. A Gen. 212 (1–2) (Apr. 2001) 17–60, https://doi.org/10.1016/S0926-860X(00)00843-7.

[18] M. Sadeqzadeh, S. Chambrey, J. Hong, P. Fongarland, F. Luck, D. Curulla-Ferré, D. Schweich, J. Bousquet, A.Y. Khodakov, Effect of different reaction conditions on the deactivation of alumina-supported cobalt Fischer-Tropsch catalysts in a milli-fixed-bed reactor: Experiments and modeling, Ind. Eng. Chem. Res. 53 (17) (2014) 6913–6922, https://doi.org/10.1021/ie4040303.

[19] A.M. Saib, D.J. Moodley, I.M. Ciobîc, M.M. Hauman, B.H. Sigwebela, C.J. Weststrate, J.W. Niemantsverdriet, J. Van De Loosdrecht, Fundamental understanding of deactivation and regeneration of cobalt Fischer-Tropsch synthesis catalysts, Catal. Today 154 (3–4) (2010) 271–282, https://doi.org/10.1016/j.cattod.2010.02.008.

[20] M. Rahmati, M.S. Safdari, T.H. Fletcher, M.D. Argyle, C.H. Bartholomew, Chemical and Thermal Sintering of Supported Metals with Emphasis on Cobalt Catalysts during Fischer-Tropsch Synthesis, Chem. Rev. 120 (10) (May 27, 2020.) 4455–4533, https://doi.org/10.1021/acs.chemrev.9b00417.

[21] M. Claeys, M.E. Dry, E. van Steen, P.J. van Berge, S. Booyens, R. Crous, P. van Helden, J. Labuschagne, D.J. Moodley, A.M. Saib, Impact of Process Conditions on the Sintering Behavior of an Alumina-Supported Cobalt Fischer-Tropsch Catalyst Studied with an in Situ Magnetometer, ACS Catal. 5 (2) (Feb. 2015) 841–852, https://doi.org/10.1021/cs501810y.

[22] M.D. Argyle, T.S. Frost, C.H. Bartholomew, Cobalt fischer-tropsch catalyst deactivation modeled using generalized power law expressions, Top. Catal. 57 (6–9) (2014) 415–429, https://doi.org/10.1007/s11244-013-0197-9.

[23] A. Carvalho, V.V. Ordomsky, Y. Luo, M. Marinova, A.R. Muniz, N.R. Marcilio, A.Y. Khodakov, Elucidation of deactivation phenomena in cobalt catalyst for Fischer-Tropsch synthesis using SSITKA, J. Catal. 344 (2016) 669–679, https://doi.org/10.1016/j.jcat.2016.11.001.

[24] B. Ernst, S. Libs, P. Chaumette, A. Kiennemann, Preparation and characterization of Fischer-Tropsch active Co/SiO_2 catalysts, Appl. Catal. A Gen. 186 (1–2) (1999) 145–168, https://doi.org/10.1016/S0926-860X(99)00170-2.

[25] H. Karaca, J. Hong, P. Fongarland, P. Roussel, A. Griboval-Constant, M. Lacroix, K. Hortmann, O.V. Safonova, A.Y. Khodakov, In situ XRD investigation of the evolution of alumina-supported cobaltcatalysts under realistic conditions of Fischer-Tropsch synthesis, Chem. Commun. 46 (5) (2010) 788–790, https://doi.org/10.1039/B920110F.

[26] A. Rochet, V. Moizan, F. Diehl, C. Pichon, V. Briois, Quick-XAS and Raman operando characterisation of a cobalt alumina-supported catalyst under realistic Fischer-Tropsch reaction conditions, Catal. Today 205 (2013) 94–100, https://doi.org/10.1016/j.cattod.2012.08.021.

[27] T.O. Eschemann, K.P. de Jong, Deactivation Behavior of Co/TiO_2 Catalysts during Fischer-Tropsch Synthesis, ACS Catal. 5 (6) (Jun. 2015) 3181–3188, https://doi.org/10.1021/acscatal.5b00268.

[28] T.O. Eschemann, J.H. Bitter, K.P. De Jong, Effects of loading and synthesis method of titania-supported cobalt catalysts for Fischer-Tropsch synthesis, Catal. Today 228 (2014) 89–95, https://doi.org/10.1016/j.cattod.2013.10.041.

[29] C.E. Kliewer, S.L. Soled, G. Kiss, Morphological transformations during Fischer-Tropsch synthesis on a titania-supported cobalt catalyst, Catal. Today 323 (Feb. 2019) 233–256, https://doi.org/10.1016/j.cattod.2018.05.021.

[30] M. Mehrbod, M. Martinelli, A.G. Martino, D.C. Cronauer, A. Jeremy Kropf, C.L. Marshall, G. Jacobs, Fischer-Tropsch synthesis: Direct cobalt nitrate reduction of promoted Co/TiO_2 catalysts, Fuel 245 (February) (Jun. 2019) 488–504, https://doi.org/10.1016/j.fuel.2019.02.083.

[31] S.J. Tauster, S.C. Fung, R.L. Garten, Strong metal-support interactions. Group 8 noble metals supported on titanium dioxide, J. Am. Chem. Soc. 100 (1) (Jan. 1978) 170–175, https://doi.org/10.1021/ja00469a029.

[32] S.J. Tauster, S.C. Fung, R.T.K. Baker, J.A. Horsley, Strong Interactions in Supported-Metal Catalysts, Science (80-.) 211 (4487) (Mar. 1981) 1121–1125, https://doi.org/10.1126/science.211.4487.1121.

[33] H. Karaca, O.V. Safonova, S. Chambrey, P. Fongarland, P. Roussel, A. Griboval-Constant, M. Lacroix, A.Y. Khodakov, Structure and catalytic performance of Pt-promoted alumina-supported cobalt catalysts under realistic conditions of Fischer-Tropsch synthesis, J. Catal. 277 (1) (Jan. 2011) 14–26, https://doi.org/10.1016/j.jcat.2010.10.007.

[34] G.L. Bezemer, T.J. Remans, A.P. van Bavel, A.I. Dugulan, Direct Evidence of Water-Assisted Sintering of Cobalt on Carbon Nanofiber Catalysts during Simulated Fischer–Tropsch Conditions Revealed with in Situ Mössbauer Spectroscopy, J. Am. Chem. Soc. 132 (25) (Jun. 2010) 8540–8541, https://doi.org/10.1021/ja103002k.

[35] L.M. van Koppen, A. Iulian Dugulan, G. Leendert Bezemer, E.J.M. Hensen, Sintering and carbidization under simulated high conversion on a cobalt-based Fischer-Tropsch catalyst; manganese oxide as a structural promotor, J. Catal. 413 (Sep. 2022) 106–118, https://doi.org/10.1016/j.jcat.2022.06.020.

[36] M.W.J. Crajé, A.M. Van der Kraan, J. Van de Loosdrecht, P.J. Van Berge, The application of Mössbauer emission spectroscopy to industrial cobalt based Fischer-Tropsch catalysts, Catal. Today 71 (3–4) (2002) 369–379, https://doi.org/10.1016/S0920-5861(01)00464-3.

[37] Z. Klencsár, MossWinn—methodological advances in the field of Mössbauer data analysis, Hyperfine Interact. 217 (1–3) (Apr. 2013) 117–126, https://doi.org/10.1007/s10751-012-0732-2.

[38] J.A. Tjon, M. Blume, Mössbauer Spectra in a Fluctuating Environment II. Randomly Varying Electric Field Gradients, Phys. Rev. 165 (2) (Jan. 1968) 456–461, https://doi.org/10.1103/PhysRev.165.456.

[39] T.W. van Deelen, J.J. Nijhuis, N.A. Krans, J. Zečević, K.P. de Jong, Preparation of Cobalt Nanocrystals Supported on Metal Oxides To Study Particle Growth in Fischer-Tropsch Catalysts, ACS Catal. 8 (11) (Nov. 2018) 10581–10589, https://doi.org/10.1021/acscatal.8b03094.

[40] T. Ohno, K. Sarukawa, K. Tokieda, M. Matsumura, Morphology of a TiO_2 Photocatalyst (Degussa, P-25) Consisting of Anatase and Rutile Crystalline Phases, J. Catal. 203 (1) (Oct. 2001) 82–86, https://doi.org/10.1006/jcat.2001.3316.

[41] M. Voß, D. Borgmann, G. Wedler, Characterization of Alumina, Silica, and Titania Supported Cobalt Catalysts, J. Catal. 212 (1) (Nov. 2002) 10–21, https://doi.org/10.1006/jcat.2002.3739.

[42] G.K. Wertheim, Hyperfine Structure of Divalent and Trivalent Fe^{57} in Cobalt Oxide, Phys. Rev. 124 (3) (Nov. 1961) 764–767, https://doi.org/10.1103/PhysRev.124.764.

[43] G.K. Wertheim, Chemical effects of nuclear transformations in Moessbauer spectroscopy, Acc. Chem. Res. 4 (11) (Nov. 1971) 373–379, https://doi.org/10.1021/ar50047a003.

[44] H. Pollak, Fe^{3+} ion Lifetime in CoO Deduced from the Auger and Mössbauer Effects, Phys. status solidi 2 (6) (1962) 720–724, https://doi.org/10.1002/pssb.19620020609.

[45] A. Cruset, J.M. Friedt, Mössbauer study of the valence state of ^{57}Fe after ^{57}Co decay in $CoFe_2O_4$, Phys. Status Solidi 45 (1) (May 1971) 189–193, https://doi.org/10.1002/pssb.2220450120.

[46] C. Wivel, B.S. Clausen, R. Candia, S. Mørup, H. Topsøe, Mössbauer Emission Studies of Calcined Co-Mo/Al_2O_3 Catalysts: Catalytic Significance of Co Precursors, J. Catal. 87 (2) (Jun. 1984) 497–513, https://doi.org/10.1016/0021-9517(84)90210-0.
[47] H. Topsoe, B.S. Clausen, R. Candia, C. Wivel, S. Mørup, In situ Mossbauer emission spectroscopy studies of unsupported and supported sulfided Co-Mo hydrodesulfurization catalysts: Evidence for and nature of a Co-Mo-S phase, J. Catal. 68 (2) (1981) 433–452, https://doi.org/10.1016/0021-9517(81)90114-7.
[48] J.A.R. Van Veen, E. Gerkema, A.M. Van Der Kraan, P.A.J.M. Hendriks, H. Beens, A ^{57}CO Mössbauer emission spectrometric study of some supported CoMo hydrodesulfurization catalysts, J. Catal. 133 (1) (Jan. 1992) 112–123, https://doi.org/10.1016/0021-9517(92)90189-O.
[49] H. P. Boehm, Chemical Identification of Surface Groups, in *Advances in Catalysis*, 1966, pp. 179–274. doi: 10.1016/S0360-0564(08)60354-5.
[50] B.M. Xaba, J.P.R. de Villiers, Sintering Behavior of TiO_2 -Supported Model Cobalt Fischer-Tropsch Catalysts under H_2 Reducing Conditions and Elevated Temperature, Ind. Eng. Chem. Res. 55 (35) (Sep. 2016) 9397–9407, https://doi.org/10.1021/acs.iecr.6b02311.
[51] R.Y. Abrokwah, M.M. Rahman, V.G. Deshmane, D. Kuila, Effect of titania support on Fischer-Tropsch synthesis using cobalt, iron, and ruthenium catalysts in silicon-microchannel microreactor, Mol. Catal. 478 (Nov. 2019), https://doi.org/10.1016/j.mcat.2019.110566.
[52] M. Wolf, E.K. Gibson, E.J. Olivier, J.H. Neethling, C.R.A. Catlow, N. Fischer, M. Claeys, Water-Induced Formation of Cobalt-Support Compounds under Simulated High Conversion Fischer-Tropsch Environment, ACS Catal. 9 (6) (Jun. 2019) 4902–4918, https://doi.org/10.1021/acscatal.9b00160.
[53] C. Lancelot, V.V. Ordomsky, O. Stéphan, M. Sadeqzadeh, H. Karaca, M. Lacroix, D. Curulla-Ferré, F. Luck, P. Fongarland, A. Griboval-Constant, A.Y. Khodakov, Direct Evidence of Surface Oxidation of Cobalt Nanoparticles in Alumina-Supported Catalysts for Fischer-Tropsch Synthesis, ACS Catal. 4 (12) (Dec. 2014) 4510–4515, https://doi.org/10.1021/cs500981p.
[54] A. Beck, H. Frey, M. Becker, L. Artiglia, M.G. Willinger, J.A. van Bokhoven, Influence of Hydrogen Pressure on the Structure of Platinum-Titania Catalysts, J. Phys. Chem. C 125 (41) (Oct. 2021) 22531–22538, https://doi.org/10.1021/acs.jpcc.1c05939.
[55] A. Beck, P. Rzepka, K.P. Marshall, D. Stoian, M.G. Willinger, J.A. van Bokhoven, Hydrogen Interaction with Oxide Supports in the Presence and Absence of Platinum, J. Phys. Chem. C 126 (41) (Oct. 2022) 17589–17597, https://doi.org/10.1021/acs.jpcc.2c05478.
[56] S. Wendt, R. Schaub, J. Matthiesen, E.K. Vestergaard, E. Wahlström, M.D. Rasmussen, P. Thostrup, L.M. Molina, E. Lægsgaard, I. Stensgaard, B. Hammer, F. Besenbacher, Oxygen vacancies on TiO_2(110) and their interaction with H_2O and O_2: A combined high-resolution STM and DFT study, Surf. Sci. 598 (1–3) (Dec. 2005) 226–245, https://doi.org/10.1016/j.susc.2005.08.041.
[57] M. Henderson, The interaction of water with solid surfaces: fundamental aspects revisited, Surf. Sci. Rep. 46 (1–8) (May 2002) 1–308, https://doi.org/10.1016/S0167-5729(01)00020-6.
[58] P.A. Thiel, T.E. Madey, The interaction of water with solid surfaces: Fundamental aspects, Surf. Sci. Rep. 7 (6–8) (Oct. 1987) 211–385, https://doi.org/10.1016/0167-5729(87)90001-X.
[59] C. Qiu, Y. Odarchenko, Q. Meng, S. Xu, I. Lezcano-Gonzalez, P. Olalde-Velasco, F. Maccherozzi, L. Zanetti-Domingues, M. Martin-Fernandez, A.M. Beale, Resolving the Effect of Oxygen Vacancies on Co Nanostructures Using Soft XAS/X-PEEM, ACS Catal. 12 (15) (Aug. 2022) 9125–9134, https://doi.org/10.1021/acscatal.2c00611.
[60] M. Wolf, N. Fischer, M. Claeys, Water-induced deactivation of cobalt-based Fischer-Tropsch catalysts, Nat. Catal. 3 (12) (Dec. 2020) 962–965, https://doi.org/10.1038/s41929-020-00534-5.
[61] H.J. Lipkin, Some simple features of the Mossbauer effect, Ann. Phys. (N. Y) 18 (2) (May 1962) 182–197, https://doi.org/10.1016/0003-4916(62)90066-0.
[62] K. Shun, K. Mori, S. Masuda, N. Hashimoto, Y. Hinuma, H. Kobayashi, H. Yamashita, Revealing hydrogen spillover pathways in reducible metal oxides, Chem. Sci. 13 (27) (2022) 8137–8147, https://doi.org/10.1039/D2SC00871H.
[63] S.-W. Ho, Surface Hydroxyls and Chemisorbed Hydrogen on Titania and Titania Supported Cobalt, J. Chinese Chem. Soc. 43 (2) (Apr. 1996) 155–163, https://doi.org/10.1002/jccs.199600023.
[64] J.D. Cashion, E.R. Vance, D.H. Ryan, Mössbauer study of the temperature dependence of electron delocalization in mixed valence freudenbergite, J. Am. Ceram. Soc. 103 (10) (Sep. 2020) 5496–5501, https://doi.org/10.1111/jace.17190.
[65] R. Riva, H. Miessner, R. Vitali, G. Del Piero, Metal–support interaction in Co/SiO_2 and Co/TiO_2, Appl. Catal. A Gen. 196 (1) (Mar. 2000) 111–123, https://doi.org/10.1016/S0926-860X(99)00460-3.
[66] T. Petsi, G.D. Panagiotou, C.S. Garoufalis, C. Kordulis, P. Stathi, Y. Deligiannakis, A. Lycourghiotis, K. Bourikas, Interfacial Impregnation Chemistry in the Synthesis of Cobalt Catalysts Supported on Titania, Chem. - A Eur. J. 15 (47) (Dec. 2009) 13090–13104, https://doi.org/10.1002/chem.200900760.
[67] K.K.B. Duff, L. Spanu, N.D.M. Hine, Impact of Carbonyl Formation on Cobalt Ripening over Titania Surface, J. Phys. Chem. C 121 (29) (Jul. 2017) 15880–15887, https://doi.org/10.1021/acs.jpcc.7b05371.
[68] E. Rytter, Ø. Borg, N.E. Tsakoumis, A. Holmen, Water as key to activity and selectivity in Co Fischer-Tropsch synthesis: γ-alumina based structure-performance relationships, J. Catal. 365 (2018) 334–343, https://doi.org/10.1016/j.jcat.2018.07.003.
[69] E. Rytter, A. Holmen, Perspectives on the Effect of Water in Cobalt Fischer-Tropsch Synthesis, ACS Catal. 7 (8) (2017) 5321–5328, https://doi.org/10.1021/acscatal.7b01525.
[70] W. Chen, R. Pestman, B. Zijlstra, I.A.W. Filot, E.J.M. Hensen, Mechanism of Cobalt-Catalyzed CO Hydrogenation: 1. Methanation, ACS Catal. 7 (12) (Dec. 2017) 8050–8060, https://doi.org/10.1021/acscatal.7b02757.
[71] R. Pestman, W. Chen, E. Hensen, Insight into the Rate-Determining Step and Active Sites in the Fischer-Tropsch Reaction over Cobalt Catalysts, ACS Catal. 9 (5) (May 2019) 4189–4195, https://doi.org/10.1021/acscatal.9b00185.